

See discussions, stats, and author profiles for this publication at: <https://www.researchgate.net/publication/260215646>

Macromolecular Metallurgy of Binary Mesocrystals via Designed Multiblock Terpolymers

ARTICLE in JOURNAL OF THE AMERICAN CHEMICAL SOCIETY · FEBRUARY 2014

Impact Factor: 12.11 · DOI: 10.1021/ja412760k · Source: PubMed

CITATIONS

9

READS

26

6 AUTHORS, INCLUDING:



Meijiao Liu

Fudan University

7 PUBLICATIONS 48 CITATIONS

SEE PROFILE



Hanlin Deng

Fudan University

3 PUBLICATIONS 13 CITATIONS

SEE PROFILE



Feng Jian Qiu

China University of Geosciences (Beijing)

136 PUBLICATIONS 2,318 CITATIONS

SEE PROFILE



An-Chang Shi

McMaster University

232 PUBLICATIONS 3,595 CITATIONS

SEE PROFILE

Macromolecular Metallurgy of Binary Mesocrystals via Designed Multiblock Terpolymers

Nan Xie,^{†,‡} Meijiao Liu,^{†,‡} Hanlin Deng,^{†,‡} Weihua Li,^{*,†} Feng Qiu,[†] and An-Chang Shi[§]

[†]State Key Laboratory of Molecular Engineering of Polymers, Department of Macromolecular Science, Fudan University, Shanghai 200433, China

[§]Department of Physics and Astronomy, McMaster University, Hamilton, Ontario, Canada, L8S 4M1

Supporting Information

ABSTRACT: Self-assembling block copolymers provide access to the fabrication of various ordered phases. In particular, the ordered spherical phases can be used to engineer soft mesocrystals with domain size at the 5–100 nm scales. Simple block copolymers, such as diblock copolymers, form a limited number of mesocrystals. However multiblock copolymers are capable to form more complex mesocrystals. We demonstrate that designed B₁AB₂CB₃ multiblock terpolymers, in which the A- and C-blocks form spherical domains and the packing of these spheres can be controlled by changing the lengths of the middle and terminal B-blocks, self-assemble into various binary mesocrystals with space group symmetries of a large number of binary ionic crystals, including NaCl, CsCl, ZnS, α -BN, AlB₂, CaF₂, TiO₂, ReO₃, Li₃Bi, Nb₃Sn(A15), and α -Al₂O₃. This approach can be generalized to other terpolymers as well as to tetrapolymers to obtain ternary mesocrystals. Our study provides a new concept of macromolecular metallurgy for producing crystal phases in a mesoscale and thus makes multiblock copolymers a robust platform for the engineering of functional materials.

Crystals are extremely attractive materials because of their rich symmetries and exceptional mechanical, electronic, and optical properties. For the fabrication of functional materials, ordered crystalline structures with feature sizes from nanometer to micrometer, which are beyond that of hard atomic crystals, are required in order to satisfy a wide range of application needs. Examples include lithographic templates of high-density magnetic storage media, quantum dots, photonic crystals, and catalysis scaffolds.^{1–4} These crystal structures can be generated by self-assembly of either nanoscale inorganic colloids^{5,6} or macromolecules, such as amphiphilic liquid crystals (LCs)^{7–11} and block copolymers (BCPs).^{12–15} Very recently, a general method of preparing DNA-programmable atom equivalents (PAEs) for achieving diverse colloidal crystals has been proposed by Zhang et al.¹⁶ Alternatively, the self-assembly of macromolecules (LCs or BCPs) provides direct access to the formation of soft mesocrystals, which are composed of spherical domains arranged on crystalline lattice. Importantly, the feature size of the mesocrystals can be readily tuned by the molecular weight of the macromolecules. On the other hand, both amphiphilic LCs and BCPs with simple molecular architectures only self-assemble into

a very limited set of crystal structures. For example, binary crystals with the symmetries of NaCl, ZnS, and AlB₂ have been obtained from inorganic colloidal systems^{5,6,17} but have not yet been obtained in BCPs. In what follows we will explore the feasibility of using designed BCPs to obtain ordered phases with symmetries of binary crystals.

It has been demonstrated that multiblock copolymers offer unparalleled opportunities for the formation of complex ordered phases. At the same time, it has been argued that multiblock copolymers could possibly become a Pandora's Box without a valid design principle of architectures because of their drastically increased phase complexity.¹⁸ Normally, polymer chemists synthesize new macromolecules and then explore into which structures they self-assemble. In view of the high dimensionality of macromolecular parameter space (e.g., chain topology, number and sequence of blocks, incompatibilities), it is more efficient to use theory and computation to derive guiding principles of rationally designed macromolecules for the formation of targeted structures. The combination of theoretical modeling and experiments can then lead to a platform of macromolecular metallurgy (MM) for recasting crystal phases with BCPs in a mesoscale.

Spherical domains self-assembled from macromolecules can be viewed as artificial macromolecular “atoms” (AMAs) (Figure 1a). These AMAs are soft, thereby having different packing mode from hard spheres which usually adopt the crystal lattice of face-centered cubic with $Fm\bar{3}m$ symmetry or hexagonal close packing (hcp) with $P6_3/mmc$ symmetry. It has been known that the simplest diblock copolymers mainly self-assemble into the body-centered cubic (bcc) phase with $Im\bar{3}m$ symmetry and only have a very tiny hcp phase region near the order–disorder transition (ODT) boundary.^{19,20} When the molecular architecture is modified to be a miktoarm star-type of AB_n with the minority A-block, another cubic phase, A15 lattice with $Pm\bar{3}n$ symmetry, becomes stable and occupies a phase region between bcc and hexagonal cylinder phase (Hex) with varying A composition.^{21,22} The A15 phase has since been found in many dendritic^{7–11} or other amphiphilic compounds.²³ In addition, a more complex noncubic sphere phase, a tetragonal lattice with a large unit cell and $P4_2/mnm$ symmetry, which was referred to as the σ phase by Frank and Kasper many years ago, has been observed in one dendritic amphiphilic compound.⁹ Recently, the σ phase has been observed in two BCP samples by Lee et al.¹⁵ Although the A15

Received: December 16, 2013

Published: February 14, 2014



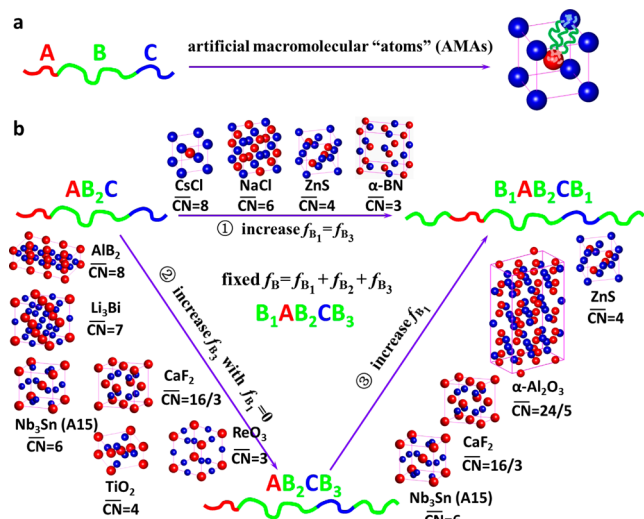


Figure 1. Design principle of multiblock terpolymers for binary soft mesocrystals. (a) AMAs self-assembled by linear ABC triblock copolymers pack into the CsCl crystal lattice. (b) AMAs formed by multiblock terpolymers can be programmed to assemble into a variety of crystallographic arrangements by tailoring the polymer architectures. Three possible paths are demonstrated as design series of mesocrystals with varying magnitude and asymmetry of coordination numbers (CNs) by tuning the relative lengths among B-blocks while keeping the total B component fixed.

and σ phases were first observed in binary transition-metal alloys,^{11,24} there is only one-component AMA in above macromolecular samples. Identification of these complex phases presents the opportunity for designing useful mesocrystals via macromolecular self-assembly.^{15,25}

Besides the one-component crystals, there are a large number of binary crystals, such as ionic crystals and binary metal alloys. These crystals provide a vast library of structure prototypes. From the perspective of both potential applications and fundamental interest, it is interesting and challenging to design mesocrystals of those structure prototypes by BCP self-assembly. In order to form binary crystals, three-component BCP is needed, in which the two minority blocks self-assemble into spheres and the majority blocks form the matrix. One of the simplest three-component BCPs is a linear ABC triblock copolymer with equal A- and C-blocks forming A and C AMAs. Theoretical studies revealed that the CsCl structure occupies most of the phase region where spheres form, and the NaCl structure is only stable in an extremely narrow range of interaction parameters, $\chi_{ij}N$ ($i, j = A, B, C$), where N is the total degree of polymerization.^{26,27} These previous studies demonstrated that the virtually limitless variations of terpolymer architectures could provide a platform to obtain various binary crystal phases. Nevertheless, a systematic approach of designing BCPs for the fabrication of diverse binary mesocrystals is required in order to prevent the system becoming a Pandora's Box.

In this report, we propose a design principle for the formation of binary mesocrystals using BCPs. The basic idea is to utilize two or more minority blocks to form the spherical domains, or AMAs, and to use the majority blocks to control the packing of the AMAs. We demonstrate the feasibility and capability of this approach by examining the phase diagram of multiblock terpolymers $B_1AB_2CB_3$, focusing on the cases where the A- and C-blocks form spheres or AMAs. The sizes and effective valencies

of the AMAs, quantified by the magnitude (or average value of CNs, \overline{CN}) and asymmetry of coordination numbers (CNs), are modulated by the relative lengths of the middle and terminal B-blocks (Figure 1b). A variety of soft binary mesocrystals with variable symmetries, along with some nonspherical phases, are predicted using the self-consistent field theory (SCFT).²⁸

There are a large number of parameters in the terpolymer systems. To reduce the parameter space as well as to make the calculations feasible, a number of parameters are kept at constant in the calculations: $\chi N = \chi_{AB}N = \chi_{BC}N = \chi_{AC}N = 80$, $f = f_A = f_C$ (volume fractions of A- and C-blocks) and equal segment sizes. Within this restricted phase space, we can divide the system into three typical cases by additional constraints: (1) symmetric-tail pentablock terpolymer with $f_{B1} = f_{B3}$ ($B_1AB_2CB_1$), (2) complete asymmetric-tail tetrablock with $f_{B1} = 0$ (AB_2CB_3), and (3) asymmetric-tail pentablock with $f_{B1} < f_{B3}$ for a given $f_A = f_C = 0.10$ ($B_1AB_2CB_3$). Accordingly, the independent controlling parameters of the first two cases are (f, f_{B2}) and that of the third case are (f_{B2}, γ) , where $\gamma = f_{B1}/f_{B3}$.

For the symmetric-tail terpolymer, $B_1AB_2CB_1$, the A- and C-spheres must pack into equivalent lattices and thus have equal CNs. The corresponding phase diagram in the f - f_{B2} plane is presented in Figure 2. The transition points are determined by

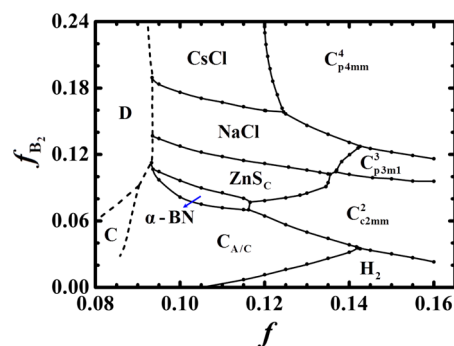


Figure 2. Phase diagram in the f - f_{B2} plane for symmetric-tail $B_1AB_2CB_1$ terpolymers with fixed $\chi N = 80$. The filled circles denote the points where we have calculated the phase boundaries, and the solid lines are a guide for the eyes. The dashed lines indicate the estimated order-disorder transition boundaries.

comparison of the free energy of the different phases, which is obtained from SCFT calculations using the pseudospectral method^{29,30} together with Anderson mixing iteration-accelerating scheme.³¹ The calculation details are given in the Supporting Information (SI). For increasing f_{B1} or decreasing f_{B2} at a fixed $f = 0.10$ along the path 1 in Figure 1b, a phase transition sequence of CsCl, NaCl, ZnS sphalerite (ZnS_C), layered honeycomb structure of α -BN, and hexagonal cylinders consisting A/C alternative domains ($C_{A/C}$) is predicted by the SCFT. Some of the ordered phases are nonspherical phases. Obviously the CNs of these mesocrystals decrease along this path (symmetries and CNs are listed in Table S1). In the α -BN structure, the A- and C-spheres are alternatively stacked along the direction normal to layers, within which each A- or C-sphere is triply coordinated by their counterparts. Between the layers, there are rarely bridges formed by the short B_2 -block. Therefore α -BN has an effective CN = 3. This structure is analogous to the graphite structure if the bridging interaction is viewed as a covalent bond and the weak nonbridging interaction is viewed as van der Waals interaction. The stable phase of the $B_1AB_2CB_1$ terpolymers is CsCl when f_{B1} is negligibly small.^{26,27} The polyhedral shape of

the Voronoi cell of the crystal with a higher CN deviates less from ideal sphere and thus has more favorable interfacial energy (see Figure S2).²¹ The advantage of interfacial energy falls off when the spherical domain shrinks. As f_{B2} decreases, the A-C spheres are pulled closer and closer (shown in Figure S4), and the sphere size is decreased because of the volume conservation. Smaller spherical domains containing less polymer chains result in higher interfacial energy. Because the sphere size in the crystal lattice with a higher CN is smaller for a given sphere–sphere distance, l_{AC} , and drops down more rapidly (more details are presented in SI), the penalty of interfacial energy is more severe in CsCl than NaCl (see Figure S1b). As a result, the CsCl structure transfers to NaCl when the B_2 -block is reduced below 0.18. Meanwhile, the sequence of transitions is accompanied by a release of stretching of the B_2 -block (see Figure S3). A similar phase sequence with decreasing tendency of CNs is shown in the two-dimensional cylindrical phase region, where the transition sequence is C_{p4mm}^4 with CN = 4, C_{p3m1}^3 with CN = 3, C_{c2mm}^2 , and a hexagonally packed double-strand helical phase H_2 , within which each helix is composed of a pair of A/C strands twining around each other (see Table S1). H_2 is different from the helical structure formed in frustrated ABC terpolymers, where two B-formed cylinders twine around a central C cylinder.³² These results lead us to conclude that the length of the middle B-block can be used to control the CNs of the structures. This conclusion can be used as one designing principle for the $B_1AB_2CB_3$ terpolymers.

Many binary ionic crystals or metallic alloys have unequal CNs. In the complete asymmetric-tail AB_2CB_3 terpolymers, the free end of the A-block can stay anywhere inside an A-sphere, while C-block has to keep its two junctions on the surface of the C-sphere and thus inducing an extra stretching of the C-blocks. In this case forming a smaller C-sphere than A-sphere is the only way to release this extra stretching. With $f = f_A = f_C$, the binary phases prefer to adopt more C-spheres than A-spheres, i.e., to have a larger CN of A than C. When a small B_1 -block is added to the A-end, the CN asymmetry can be reduced. The phase diagram of (f, f_{B2}) for AB_2CB_3 is given in Figure 3. Similarly, the phase sequence with declining \overline{CN} is seen in both sphere and cylinder phases when decreasing f_{B2} along the path 2 in Figure 1b. At the phase region of small f , abiding by the proposed guiding principle, there exists a phase sequence of CsCl, AlB_2 ,

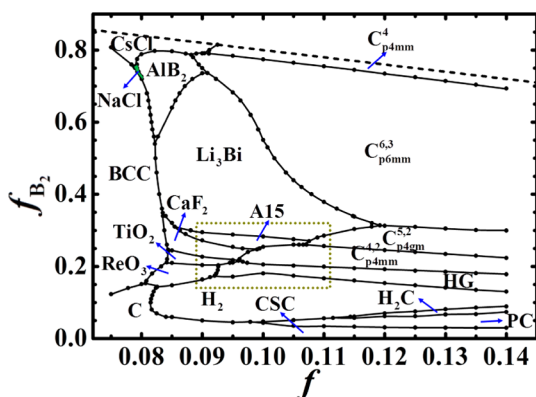


Figure 3. Phase diagram in the f – f_{B2} plane for AB_2CB_3 terpolymers with fixed $\chi N = 80$. The top dashed line indicates the limit of AB_2C triblock. The very tiny NaCl region is filled with green color. Here bcc and C represent the simple bcc sphere and hexagonal cylinder phases, respectively, where A- and C-blocks do not phase separate. The portion inside the dotted line box is enlarged in Figure S7.

$C_{p6mm}^{6.3}$, Li_3Bi , Nb_3Sn (A15), CaF_2 , TiO_2 , ReO_3 , helical supercylinder H_2 , and hexagonal core–shell cylinder CSC. In the region of cylinder phases, a number of intriguing phases are obtained, including $C_{p6mm}^{6.2}$, $C_{p4gm}^{5.2}$, $C_{p4mm}^{4.2}$, perforated supercylinder PC, and hierarchical gyroid phase HG. The general sequence of cylinder phases is C_{p4mm}^4 , $C_{p6mm}^{6.3}$, $C_{p6mm}^{6.2}$ (occupying a very tiny region), $C_{p4gm}^{5.2}$, and $C_{p4mm}^{4.2}$. The $C_{p6mm}^{6.3}$ phase was first reported with a linear SBM terpolymer 15 years ago,³³ and it was re-identified precisely by a resonant soft X-ray scattering with a linear IS2VP terpolymer.³⁴ In fact, the $C_{p6mm}^{6.3}$ phase is not a stable phase in the simple ABC terpolymer with the present parameters. However, when a slight asymmetry is introduced by adding a small B-block onto the end of C-block to form ABCB tetrablock, $C_{p6mm}^{6.3}$ occupies a significant phase region at the cost of the C_{p4mm}^4 structure. These two-dimensional cylindrical morphologies with symmetries of $p4mm$, $p6mm$, and $p4gm$, have been observed in bolaamphiphilic LCs with a lateral chain, where the pattern symmetry is simply modulated by the length of lateral chain.³⁵ The predominant factor in the two systems is fairly similar, i.e., to fill the outside space of spheres under the framework of crystal lattices with a given lattice constant using varying amount of matter (end blocks or lateral chains). Based on these results, we can also design interesting series of mesocrystals when one or a few lateral B-blocks are used to replace the end blocks.

There are two competing factors in phase transitions: the average magnitude of CNs determined by the length of the middle B_2 -block and the asymmetric degree of CNs depending on the architecture asymmetry. The symmetric and asymmetric terpolymers discussed above are two limits. On the other hand, the asymmetric degree can be varied continuously by modifying the relative lengths of the two end B-blocks in $B_1AB_2CB_3$, which allows us to examine the change of CNs from symmetric to asymmetric. The phase diagram in the (f_{B2}, γ) plane for fixed $f = 0.10$ is given in Figure 4. The path 3 in Figure 1b, along which the

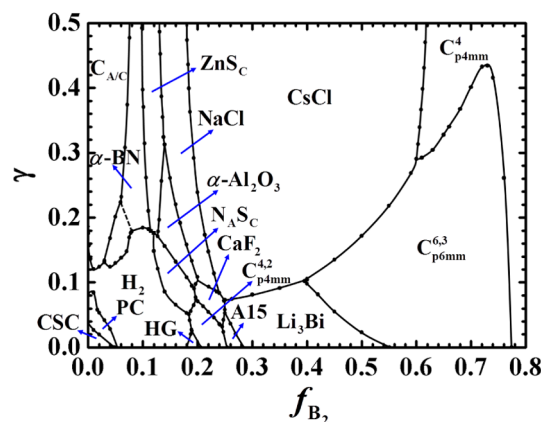


Figure 4. Phase diagram as function of f_{B2} and $\gamma = f_{B1}/f_{B3}$ for $B_1AB_2CB_3$ pentablock terpolymers with fixed $\chi N = 80$ and $f = 0.10$. α -BN at the bottom of the region transforms continuously into a new phase (denoted as α -nBN in Table S1) by fusing isolated A domains into layered network when the molecular asymmetry is added, and therefore the transition curve is plotted with dashed lines.

phase sequence with decreasing \overline{CN} and CN asymmetry is comprised of A15, CaF_2 , α - Al_2O_3 , and ZnS_C , is identified in this phase diagram. One notable intriguing feature is that the complex phase of rhombohedral α - Al_2O_3 corundum becomes stable and has a noticeable region of $0.1 \lesssim \gamma \lesssim 0.32$ locating between the ZnS_C and NaCl structures. This indicates that the asymmetric

degree of CN is much smaller than that between two end blocks because one-dimensional chains are packed into three-dimensional domains. Additionally, the presence of the α -Al₂O₃ structure foretells the possibility of a new binary cylinder pattern with a small CN asymmetry of 2:3 if varying γ in the phase region of cylinders. Besides sphere crystals, a few new phases like N_ASC and α -nBN are identified (see Table S1).

In summary, the current study demonstrates a simple valid principle for the fabrication of binary mesocrystalline phases via the self-assembly of multiblock B₁AB₂CB₃ terpolymers, in which the middle B-block is used to control the coordination number and size of the A and C spherical domains. At the same time, the end B-blocks are introduced to ensure a fixed total B composition on the one hand and to modulate the asymmetric degree of CNs via varying their relative lengths on the other hand. This design principle can be generalized to the fabrication of ternary mesocrystals using multiblock tetrapolymers. This theoretical study presented in this paper serves as a starting point for the establishment of a platform for the macromolecular metallurgy of mesocrystals via the self-assembly of multiblock copolymers. At the same time, the current study provides a compelling example in which multiblock copolymers can be considered more likely a panacea than a Pandora's Box in materials design.¹⁸ With the development of precise synthesis techniques, more complex multiblock terpolymers have been synthesized, such as the VISISISIV undecablock,³⁶ CECEC-P hexablock,³⁷ and SISO tetrablock terpolymers.^{15,38} In particular, the SISO tetrablock terpolymer is quite similar to the complete asymmetric-tail terpolymer sample when the composition of PI block is reduced to form spheres. The availability of these complex multiblock copolymers makes it possible to explore the theoretically predicted crystal phases by experiments.

■ ASSOCIATED CONTENT

■ Supporting Information

Theoretical methods, Tables S1–S4, and Figures S1–S7. This material is available free of charge via the Internet at <http://pubs.acs.org>.

■ AUTHOR INFORMATION

Corresponding Author

weihuali@fudan.edu.cn

Author Contributions

[‡]These authors contributed equally.

Notes

The authors declare no competing financial interest.

■ ACKNOWLEDGMENTS

This work is supported by NSFC (21322407, 21174031); the National Basic Research Program of China (2011CB605702).

■ REFERENCES

- (1) Park, M.; Harrison, C.; Chaikin, P. M.; Register, R. A.; Adamson, D. H. *Science* **1997**, 276, 1401.
- (2) Chan, V. Z. H.; Hoffman, J.; Lee, V. Y.; Iatrou, H.; Avgeropoulos, A.; Hadjichristidis, N.; Miller, R. D.; Thomas, E. L. *Science* **1999**, 286, 1716.
- (3) Thurn-Albrecht, T.; Schotter, J.; Kastle, C. A.; Emley, N.; Shibauchi, T.; Krusin-Elbaum, L.; Guarini, K.; Black, C. T.; Tuominen, M. T.; Russell, T. P. *Science* **2000**, 290, 2126.
- (4) Lopes, W. A.; Jaeger, H. M. *Nature* **2001**, 414, 735.
- (5) Vermolen, E. C. M.; Kuijk, A.; Filion, L. C.; Hermes, M.; Thijssen, J. H. J.; Dijkstra, M.; van Blaaderen, A. *Proc. Natl. Acad. Sci. U.S.A.* **2009**, 106, 16063.
- (6) Dong, A. G.; Chen, J.; Vora, P. M.; Kikkawa, J. M.; Murray, C. B. *Nature* **2010**, 466, 474.
- (7) Hudson, S.; Jung, H.-T.; Percec, V.; Cho, W.-D.; Johansson, G.; Ungar, G.; Balagurusamy, V. *Science* **1997**, 278, 449.
- (8) Percec, V.; Ahn, C.-H.; Ungar, G.; Yeardley, D.; Möller, M.; Sheiko, S. *Nature* **1998**, 391, 161.
- (9) Ungar, G.; Liu, Y.; Zeng, X.; Percec, V.; Cho, W.-D. *Science* **2003**, 299, 1208.
- (10) Percec, V.; Mitchell, C. M.; Cho, W.-D.; Uchida, S.; Glodde, M.; Ungar, G.; Zeng, X.; Liu, Y.; Balagurusamy, V. S.; Heiney, P. A. *J. Am. Chem. Soc.* **2004**, 126, 6078.
- (11) Ungar, G.; Zeng, X. *Soft Matter* **2005**, 1, 95.
- (12) Hillmyer, M. A.; Bates, F. S.; Almdal, K.; Mortensen, K.; Ryan, A. J.; Fairclough, J. P. A. *Science* **1996**, 271, 976.
- (13) Hamley, I. W. *The Physics of Block Copolymers*; Oxford Univ. Press: Oxford, 1998.
- (14) Bang, J.; Jeong, U.; Ryu, D. Y.; Russell, T. P.; Hawker, C. J. *Adv. Mater.* **2009**, 21, 4769.
- (15) Lee, S.; Bluemle, M. J.; Bates, F. S. *Science* **2010**, 330, 349.
- (16) Zhang, C.; Macfarlane, R. J.; Young, K. L.; Choi, C. H. J.; Hao, L. L.; Auyeung, E.; Liu, G. L.; Zhou, X. Z.; Mirkin, C. A. *Nat. Mater.* **2013**, 12, 741.
- (17) Maldovan, M.; Thomas, E. L. *Nat. Mater.* **2004**, 3, 593.
- (18) Bates, F. S.; Hillmyer, M. A.; Lodge, T. P.; Bates, C. M.; Delaney, K. T.; Fredrickson, G. H. *Science* **2012**, 336, 434.
- (19) Matsen, M. W.; Schick, M. *Phys. Rev. Lett.* **1994**, 72, 2660.
- (20) Matsen, M. W. *J. Phys.: Condens. Matter* **2002**, 14, R21.
- (21) Grason, G. M.; DiDonna, B.; Kamien, R. D. *Phys. Rev. Lett.* **2003**, 91, 058304.
- (22) Grason, G. M.; Kamien, R. D. *Macromolecules* **2004**, 37, 7371.
- (23) Cheng, X. H.; Diele, S.; Tschierske, C. *Angew. Chem., Int. Ed.* **2000**, 39, 592.
- (24) Sinha, A. K. *Topologically Close Packed Structures in Transition Metal Alloys*; Pergamon Press: Oxford, 1972.
- (25) Peterca, M.; Percec, V. *Science* **2010**, 330, 333.
- (26) Matsen, M. W. *J. Chem. Phys.* **1998**, 108, 785.
- (27) Qin, J.; Bates, F. S.; Morse, D. C. *Macromolecules* **2010**, 43, 5128.
- (28) Fredrickson, G. H. *The Equilibrium Theory of Inhomogeneous Polymers*; Oxford Univ. Press: Oxford, 2006.
- (29) Rasmussen, K. ø.; Kalosakas, G. J. *Polym. Sci., Part B: Polym. Phys.* **2002**, 40, 1777.
- (30) Tzeremes, G.; Rasmussen, K. ø.; Lookman, T.; Saxena, A. *Phys. Rev. E* **2002**, 65, 041806.
- (31) Thompson, R. B.; Rasmussen, K. ø.; Lookman, T. *J. Chem. Phys.* **2004**, 120, 31.
- (32) Li, W. H.; Qiu, F.; Shi, A. C. *Macromolecules* **2012**, 45, 503.
- (33) Brinkmann, S.; Stadler, R.; Thomas, E. L. *Macromolecules* **1998**, 31, 6566.
- (34) Wang, C.; Lee, D. H.; Hexemer, A.; Kim, M. I.; Zhao, W.; Hasegawa, H.; Ade, H.; Russell, T. P. *Nano Lett.* **2011**, 11, 3906.
- (35) Tschierske, C. *Chem. Soc. Rev.* **2007**, 36, 1930.
- (36) Masuda, J.; Takano, A.; Nagata, Y.; Noro, A.; Matsushita, Y. *Phys. Rev. Lett.* **2006**, 97, 098301.
- (37) Fleury, G.; Bates, F. S. *Macromolecules* **2009**, 42, 1691.
- (38) Zhang, J.; Bates, F. S. *J. Am. Chem. Soc.* **2012**, 134, 7636.

Supplementary Materials for

Macromolecular metallurgy of binary mesocrystals via designed multiblock terpolymers

Nan Xie, Meijiao Liu, Hanlin Deng, Weihua Li, Feng Qiu, An-Chang Shi

correspondence to: weihuali@fudan.edu.cn

This PDF file includes:

Theoretical Methods

Tables S1 to S4

Detailed mechanism in the design principle

Figures S1 to S7

Theoretical Methods

We consider an incompressible melt of $B_1AB_2CB_3$ linear block terpolymers with a total degree of polymerization N in a volume of V . The lengths of the different blocks are specified by $f_{B_1}N$, $f_A N$, $f_{B_2}N$, $f_C N$, and $f_{B_3}N$ ($f_{B_1} + f_A + f_{B_2} + f_C + f_{B_3} = 1$), respectively. The interactions between the three dissimilar monomers are characterized by the product of three Flory-Huggins interaction parameters and N , $\chi_{AB}N$, $\chi_{AC}N$, and $\chi_{BC}N$. In the self-consistent field theory (SCFT) for ideal Gaussian polymer chains (28), the free energy functional in the unit of $k_B T$ (k_B is the Boltzmann constant and T is the temperature), of an incompressible melt of n identical $B_1AB_2CB_3$ polymer chains, can be expressed as

$$\begin{aligned} \frac{F}{nk_B T} = & -\ln Q + \frac{1}{V} \int d\mathbf{r} \{ \chi_{AB} N \phi_A(\mathbf{r}) \phi_B(\mathbf{r}) + \chi_{AC} N \phi_A(\mathbf{r}) \phi_C(\mathbf{r}) + \chi_{BC} N \phi_B(\mathbf{r}) \phi_C(\mathbf{r}) \\ & - w_A(\mathbf{r}) \phi_A(\mathbf{r}) - w_B(\mathbf{r}) \phi_B(\mathbf{r}) - w_C(\mathbf{r}) \phi_C(\mathbf{r}) - \xi(\mathbf{r}) [1 - \phi_A(\mathbf{r}) - \phi_B(\mathbf{r}) - \phi_C(\mathbf{r})] \} \end{aligned} \quad (S1)$$

where $\phi_A(\mathbf{r})$, $\phi_B(\mathbf{r})$ and $\phi_C(\mathbf{r})$ are the monomer densities, and the space function of $\xi(\mathbf{r})$ is a Lagrange multiplier used to enforce the incompressibility condition. The quantity Q is the partition function of a single terpolymer chain interacting with the mean fields $w_A(\mathbf{r})$, $w_B(\mathbf{r})$ and $w_C(\mathbf{r})$, which are produced by the surrounding chains. For the convenience of analyzing the mechanism of phase separation, the free energy is usually divided into two contributions, interfacial energy U and entropic energy $-TS$,

$$\begin{aligned} F &= U - TS \\ \frac{U}{nk_B T} &= \frac{1}{V} \int d\mathbf{r} [\chi_{AB} N \phi_A(\mathbf{r}) \phi_B(\mathbf{r}) + \chi_{AC} N \phi_A(\mathbf{r}) \phi_C(\mathbf{r}) + \chi_{BC} N \phi_B(\mathbf{r}) \phi_C(\mathbf{r})] \\ -\frac{S}{nk_B} &= -\ln Q - \frac{1}{V} \int d\mathbf{r} \{ w_A(\mathbf{r}) \phi_A(\mathbf{r}) + w_B(\mathbf{r}) \phi_B(\mathbf{r}) + w_C(\mathbf{r}) \phi_C(\mathbf{r}) \} \end{aligned} \quad (S2)$$

Minimization of the free energy with respect to the monomer densities and the mean fields leads to the following standard SCFT equations

$$\begin{aligned}
w_A(\mathbf{r}) &= \chi_{AB} N\phi_B(\mathbf{r}) + \chi_{AC} N\phi_C(\mathbf{r}) + \xi(\mathbf{r}) \\
w_B(\mathbf{r}) &= \chi_{AB} N\phi_A(\mathbf{r}) + \chi_{BC} N\phi_C(\mathbf{r}) + \xi(\mathbf{r}) \\
w_C(\mathbf{r}) &= \chi_{AC} N\phi_A(\mathbf{r}) + \chi_{BC} N\phi_B(\mathbf{r}) + \xi(\mathbf{r}) \\
\phi_A(\mathbf{r}) &= \frac{1}{Q} \int_{f_{B_1}}^{f_{B_1}+f_A} ds q(\mathbf{r}, s) q^\dagger(\mathbf{r}, s) \\
\phi_B(\mathbf{r}) &= \frac{1}{Q} \left\{ \int_0^{f_{B_1}} ds q(\mathbf{r}, s) q^\dagger(\mathbf{r}, s) + \int_{f_{B_1}+f_A}^{f_{B_1}+f_A+f_{B_2}} ds q(\mathbf{r}, s) q^\dagger(\mathbf{r}, s) \right. \\
&\quad \left. + \int_{1-f_{B_3}}^1 ds q(\mathbf{r}, s) q^\dagger(\mathbf{r}, s) \right\} \\
\phi_C(\mathbf{r}) &= \frac{1}{Q} \int_{f_{B_1}+f_A+f_{B_2}}^{1-f_{B_3}} ds q(\mathbf{r}, s) q^\dagger(\mathbf{r}, s) \\
\phi_A(\mathbf{r}) + \phi_B(\mathbf{r}) + \phi_C(\mathbf{r}) &= 1 \\
Q &= \frac{1}{V} \int d\mathbf{r} q(\mathbf{r}, s) q^\dagger(\mathbf{r}, s)
\end{aligned} \tag{S3}$$

In the above equations, $q(\mathbf{r}, s)$ and $q^\dagger(\mathbf{r}, s)$ are the end-segment distribution functions which satisfy the modified diffusion equations,

$$\begin{aligned}
\frac{\partial q(\mathbf{r}, s)}{\partial s} &= \nabla^2 q(\mathbf{r}, s) - w(\mathbf{r}, s) q(\mathbf{r}, s) \\
-\frac{\partial q^\dagger(\mathbf{r}, s)}{\partial s} &= \nabla^2 q^\dagger(\mathbf{r}, s) - w(\mathbf{r}, s) q^\dagger(\mathbf{r}, s)
\end{aligned} \tag{S4}$$

where $w(\mathbf{r}, s) = w_K(\mathbf{r})$ when s belongs to the K component ($K=A, B$, or C). Here the radius of gyration of the polymer chain, R_g , is used as the unit of spatial lengths. We use the pseudo-spectral method (29, 30) to solve the modified diffusion equations, and implement the Anderson mixing iteration scheme (31) to accelerate the converging speed toward SCFT solutions. To impose periodic boundary conditions to each direction, a rectangular cuboid unit is set for each phase. The utilization of this unit cell facilitates the minimization of free energy with respect to box sizes. The box is discretized into a 64^3

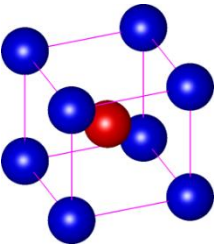
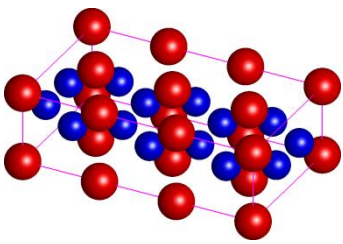
lattice, where the maximal lattice spacing is smaller than $0.2 R_g$. We use 200 points to divide the chain contour.

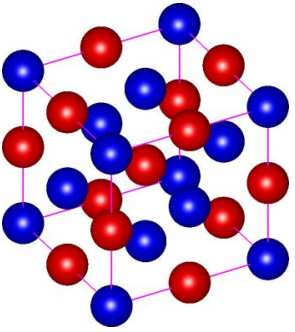
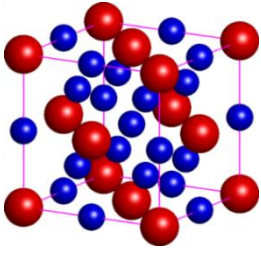
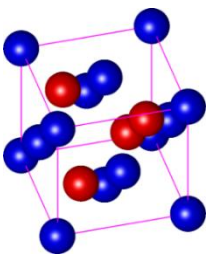
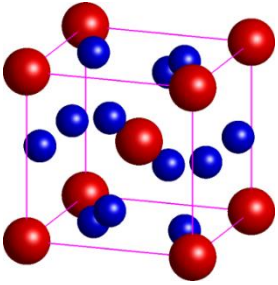
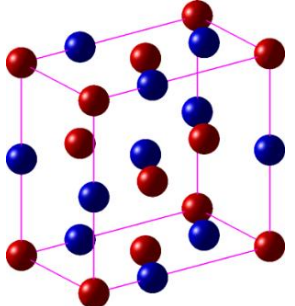
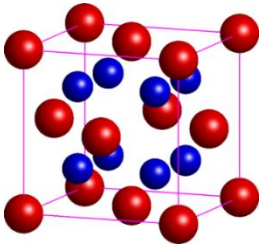
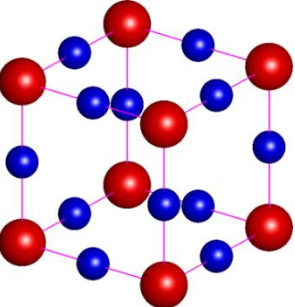
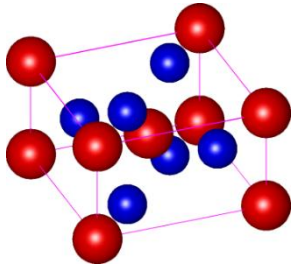
In this work, the most challenging work is to search possible solutions of the SCFT equations for the self-assembly of $B_1AB_2CB_3$ terpolymers, *i.e.*, the possible candidate phases. As our main interest is focused on the exploration of diverse binary spherical phases, we choose small lengths of A- and C-blocks to guarantee that the A- and C-blocks individually self-assemble into spherical domains immersed in the B-matrix. Then we calculate free energies of the crystal phases with the space-group symmetries of structure prototypes of a number of common inorganic crystals, such as CsCl, NaCl, ZnS_C , CaF_2 , and Li_3Bi . By comparing their stabilities, we verify the proposed design principle, *i.e.*, the dependence of the coordination numbers (CNs) or the asymmetry of coordination numbers on the varying length of the bridge B_2 -block. Finally, we investigate more SCFT solutions of other possible crystal phases with similar CNs using special initial conditions to identify the stable phases. In addition, we also consider a number of possible neighbor phases of these sphere phases, such as cylinders (core-shell, alternating, or helical) and double-network phases. In our calculations, we identify 32 candidate phases which have reasonably low free energies (Table S1-S3). Among these phases, there are 16 crystal phases resembling the structure prototypes of binary crystals each of which is denoted by the chemical formula of one of the corresponding inorganic crystals, such as CsCl, NaCl, ZnS sphalerite (ZnS_C), ZnS Wurtzite (ZnS_H), α -BN, AlB_2 , Li_3Bi , Nb_3Sn (A15), CaF_2 , TiO_2 , ReO_3 , α - Al_2O_3 , PtS, NiAs, $MgCu_2$, and Cu_3Au . Additionally, there are 9 two-dimensional cylinder phases denoted as C_x^n or $C_x^{n,m}$ where the letter C indicates the *cylinder* phase, the subscript x indicates the plane group

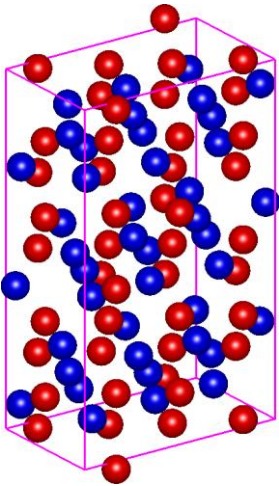
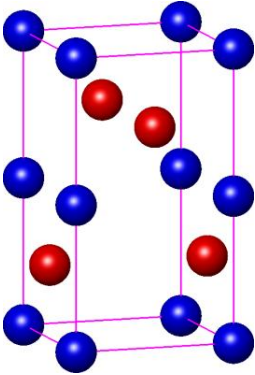
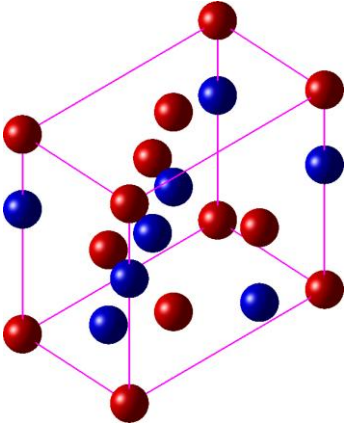
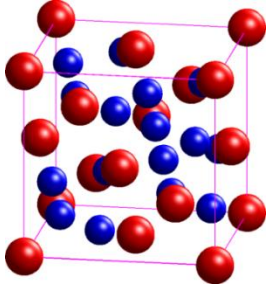
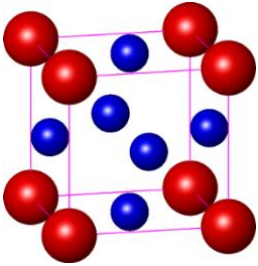
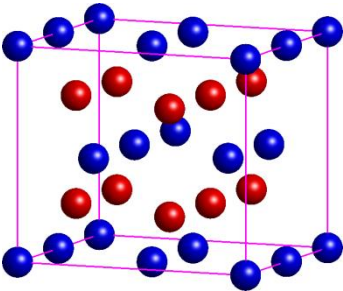
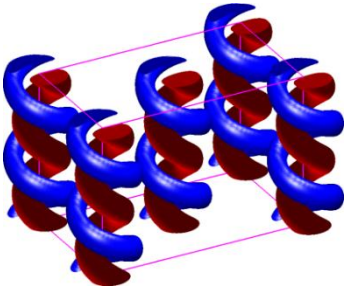
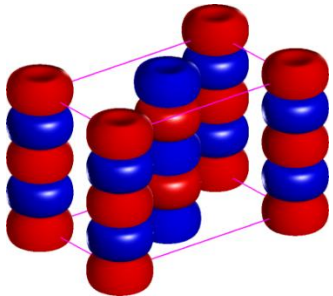
symmetry, and the superscript n or (n,m) indicates the value of symmetric or asymmetric CNs, and superscript indicates cylinder phase. The other 8 phases include helical super-cylinder phases (H_2 and H_2C), perforated super-cylinder phase (PC), A/C alternative cylinder phase ($C_{A/C}$), hierarchical gyroid phase (HG), and two new phases of α -nBN and $N_A S_C$, for which more details are provided in the description of Table S1. Besides the above binary crystal phases, other binary phases, such as PbO, SiO₂ (α -tridymite and α -cristobalite), MoS₂, and CdI₂, are also examined for some parameters, however, some of them have much higher free energies and others are not even metastable. A word of caution is that we cannot guarantee that each phase in our phase diagrams has the lowest free energy because this is a formidable task (see Ref. S1).

Table S1.

List of three-dimensional candidate phases considered in this work and their schematic plots where A- and C-domains are indicated by red and blue colors, respectively. The space group symmetry/number and the average coordination number (\overline{CN}) are also listed for each phase which is denoted by the chemical formula of one of typical inorganic crystals belonging to the same structure prototype. Note that the helical phase of H_2C , in which two C-helices twine around a *central* A-domain, is different from the helical phase of H_2 , where A- and C-helices twisting around each other. The designations HG, PC, and $C_{A/C}$ represent the hierarchical gyroid phase, the hexagonal cylinder phase where each A-cylinder is surrounded by perforated C-layer, and the hexagonal phase of cylinders composed of A/C alternative domains, respectively. The new phase of α -nBN is formed when fusing red A-spheres into layered A-network. The other new phase denoted as N_AS_C , where N_A and S_C indicate the network of A-domains and the C-spheres, respectively, is extrapolated from the phase of α -nBN, but different from the latter one. In N_AS_C , the C-domains embedded in the A-network are split into double-layer spheres located at the two sides of the A-network. Both α -nBN and N_AS_C phases have their mirror phases with exchanging A- and C-domains.

Type (Space Group)	Schematic Plot of Structure	\overline{CN}	Type (Space Group)	Schematic Plot of Structure	\overline{CN}
CsCl ($Pm\bar{3}m$, No. 221)		8	AlB₂ ($P6/mmm$, No. 191)		8

<p>NaCl ($Fm\bar{3}m$, No. 225)</p>		<p>6</p>	<p>Li₃Bi ($Fm\bar{3}m$, No. 225)</p>		<p>7</p>
<p>ZnS_C ($F\bar{4}3m$, No. 216)</p>		<p>4</p>	<p>Nb₃Sn (A15) ($Pm\bar{3}n$, No. 223)</p>		<p>6</p>
<p>α-BN ($P6_3/mmc$, No. 194)</p>		<p>3</p>	<p>CaF₂ ($Fm\bar{3}m$, No. 225)</p>		<p>$\frac{16}{3}$</p>
<p>ReO₃ ($Pm\bar{3}m$, No. 221)</p>		<p>3</p>	<p>TiO₂ ($P4_2/mnm$, No. 136)</p>		<p>4</p>

$\alpha\text{-Al}_2\text{O}_3$ $(R\bar{3}c,$ No. 167)		$\frac{24}{5}$	PtS $(P4_2/mmc,$ No. 131)		4
ZnS_H $(P6_3/mc,$ No. 186)		4	MgCu₂ $(Fd\bar{3}m,$ No. 227)		8
Cu₃Au $(Pm\bar{3}m,$ No. 221)		6	NiAs $(P6_3/mmc,$ No. 194)		6
H₂		/	C_{A/C}		/

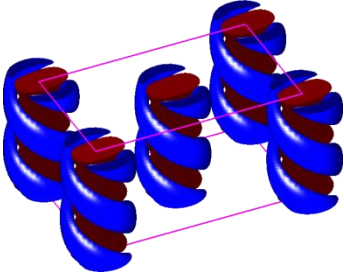
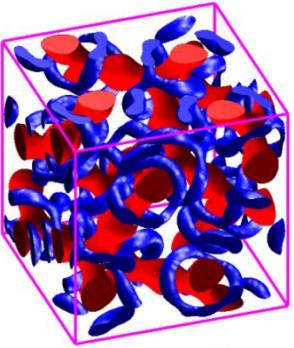
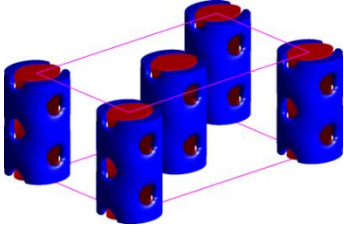
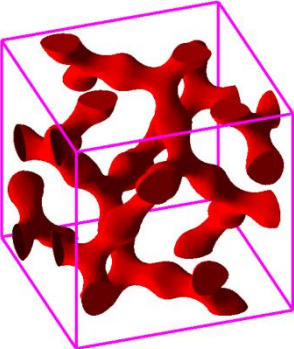
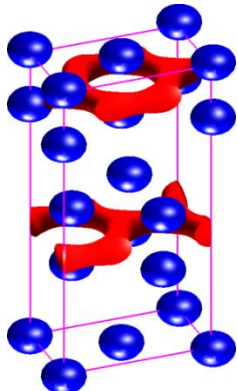
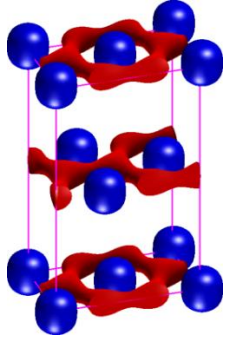
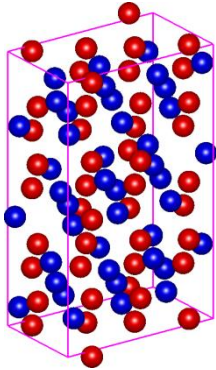
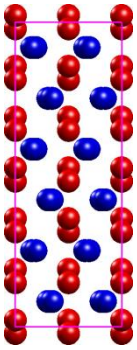
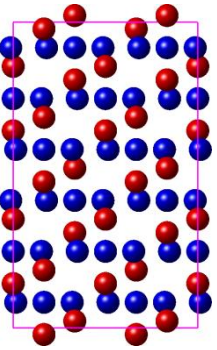
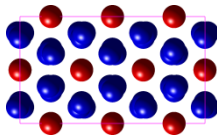
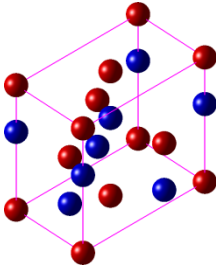
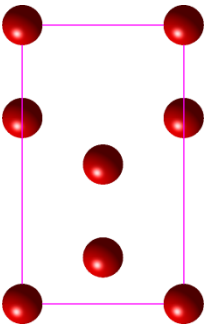
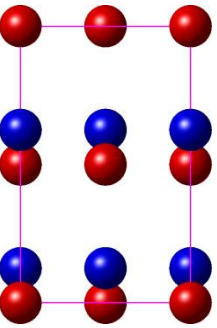
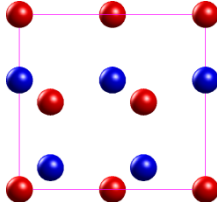
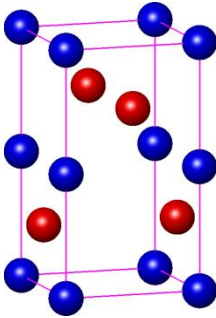
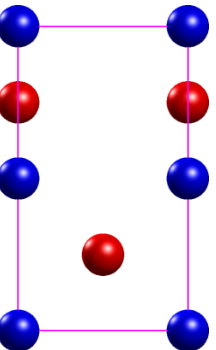
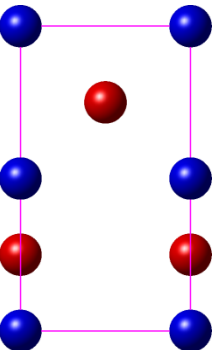
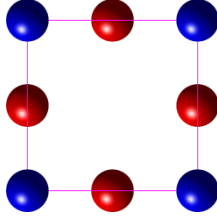
H_2C		/	HG		/
PC		/			/
$\text{N}_\text{A}\text{Sc}$		/	$\alpha\text{-nBN}$		/

Table S2.

List of projection figures in [001], [010], and [100] projection planes, for some complex crystal phases, such as α -Al₂O₃, ZnS_H, PtS, MgCu₂, NiAs, and N_AS_C.

Type	3D Plot	Projection Plane		
		[100]	[010]	[001]
α -Al ₂ O ₃				
ZnS _H				
PtS				

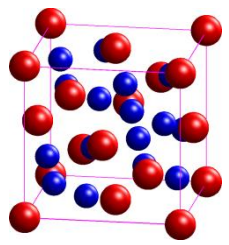
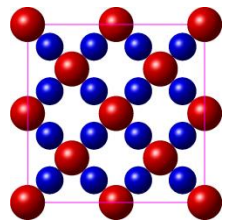
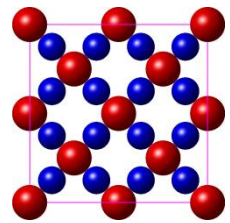
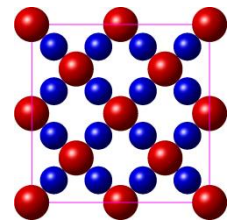
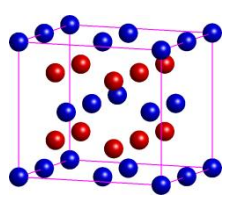
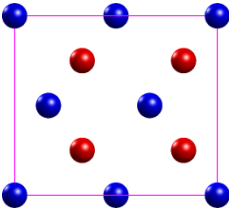
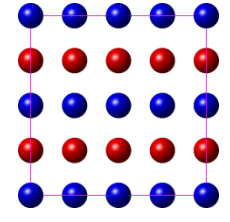
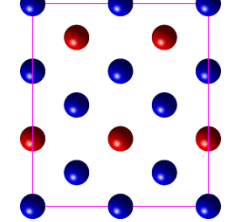
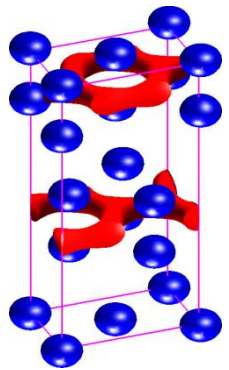
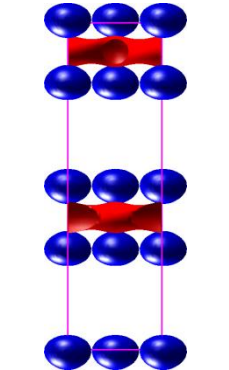
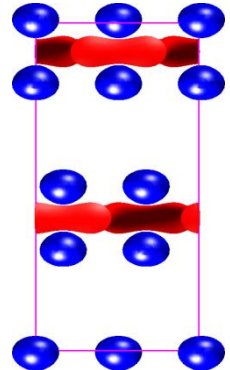
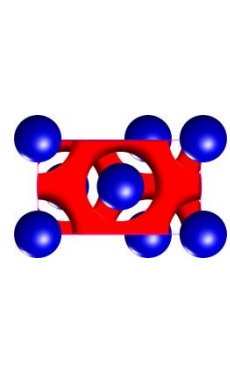
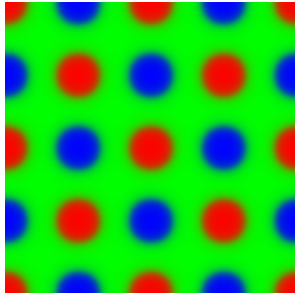
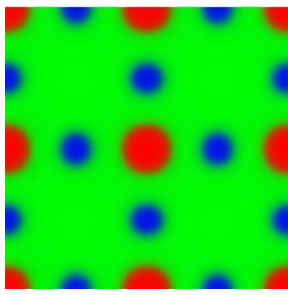
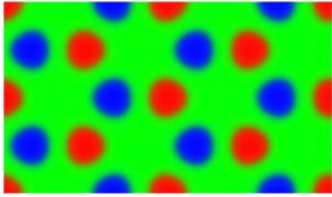
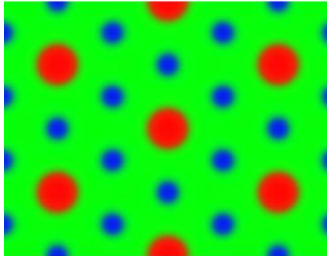
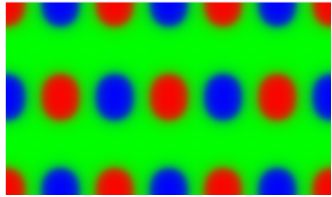
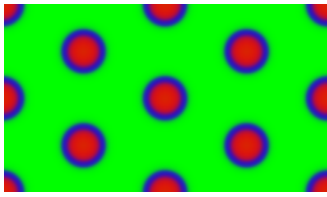
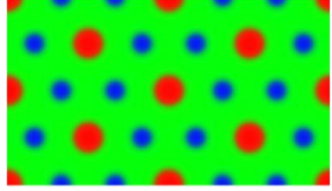
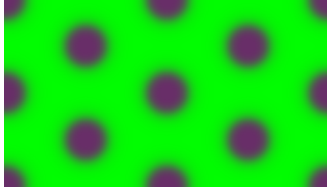
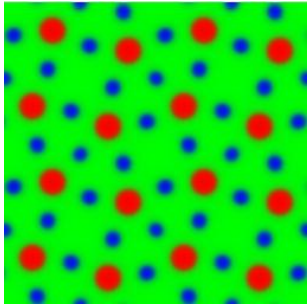
Type	3D Plot	Projection Plane		
		[100]	[010]	[001]
MgCu ₂				
NiAs				
N _A Sc				

Table S3.

List of two-dimensional morphologies observed in this work and their density plots where A, B, and C rich domains are indicated by red, green, and blue colors, respectively. The plane group symmetry and the average CN are listed for each cylinder pattern. These cylinder patterns with equal or unequal CNs are denoted as C_x^n or $C_x^{n,m}$, where x indicates the plane group symmetry and n or (n,m) indicates the equal or unequal CNs. Here $C_{p6mm}^{6,2}$ becomes stable when $f > 0.14$.

Type	Density Profile of Morphologies	\overline{CN}	Type	Density Profile of Morphologies	\overline{CN}
C_{p4mm}^4		4	$C_{p4mm}^{4,2}$		$\frac{8}{3}$
C_{p3m1}^3		3	$C_{p6mm}^{6,2}$		3
C_{c2mm}^2		2	CSH		/
$C_{p6mm}^{6,3}$		4	C		/

$C_{p4gm}^{5,2}$		$\frac{20}{7}$			
------------------	---	----------------	--	--	--

Detailed mechanism of the designing principle

Here we take the phase sequence of CsCl, NaCl, and ZnS_C in the phase diagram of Fig. 2, as an example to explain the designing mechanism how the spanning B₂-block modulates the transitions between different binary crystal phases. For the symmetric B₁AB₂CB₁ terpolymer, three equal interaction parameters and the block ratios of A and C are fixed as $\chi N = 80$ and $f = 0.10$, respectively. The free energy comparison is given in Fig. S1. When f_{B_2} is very large (the limit case is $f_{B_2} = 1 - 2f$ for the AB₂C triblock terpolymer), the stable phase is CsCl because the A/B or B/C interface, whose shape is less influenced by shape of the Voronoi cell in the crystal lattice with a higher CN, is more spherical (see Fig. S2) and thus gives rise to lower interfacial energy (see Fig. S1b). In this case, the far outside space of spheres from the A/B or B/C interface is filled with the loops formed by the middle B₂-blocks. As decreasing the length of B₂-block, f_{B_2} , the furthest space cannot be reached by the B₂-loops, and instead by the two end B-blocks. Less and less configurations for the spanning B₂ block result in more and more stretching onto the B₂-block. Fig. S3 shows $l_{AC}^* = l_{AC} / l_0$ as a function of f_{B_2} , where $l_0 = [(f_{B_2} + f)N]^{1/2}b$ is approximately the ideal end-to-end distance between the centers of A- and C-blocks. In return, this stretching enforces the A-C sphere distance of l_{AC} to be reduced, which is accompanied by the reduction of the sphere size (see Fig. S4). At the same time, the formation of smaller spheres which contain less polymer chains induces higher interfacial energy per chain because the interfacial area per chain is inversely proportional to the sphere size in the strong-segregation theory. When a delicate balance between the two factors is achieved for a given crystal phase, both the stretching degree

of the spanning B₂-block and the penalty of the interfacial energy become higher and higher as f_{B_2} decreases (see Fig. S1b and Fig. S3). However, one additional way to ease the strong competition is to alter the crystal phase into a new one with a sparser piling of spheres, *i.e.*, with a smaller CN. The relationship of $r_{A/C}$ and l_{AC} in Eqs. (S5) directly suggests that the crystal phase with lower CN gives rise to a larger sphere size for a given A-C sphere distance which benefits the interfacial energy, or oppositely, a given sphere size gives rise to a smaller l_{AC} which favors releasing the high stretching in the B₂-block. Fig. S4b obviously show that the sphere radius drops down more rapidly in the crystal phase with a higher CN, where the sphere radius is estimated under the strong-segregation approximation and the assumption that the A and C domains are ideally spherical. Therefore, in the case that the spanning B₂-block is severely stretched, the binary crystal phases with a decreasing CN become stable in sequence. This fundamental modulation mechanism in the design principle is also suitable for the self-assembly of asymmetric B₁AB₂CB₃ terpolymers.

$$r_{A/C} = \lambda \left(\frac{3f}{4\pi} \right)^{1/3} l_{AC}, \quad \lambda = \begin{cases} 2 / \sqrt{3} \approx 1.15, & \text{for CsCl} \\ 2 / 4^{1/3} \approx 1.26, & \text{for NaCl} \\ 4^{2/3} / \sqrt{3} \approx 1.45, & \text{for ZnS}_C \end{cases} \quad (\text{S5})$$

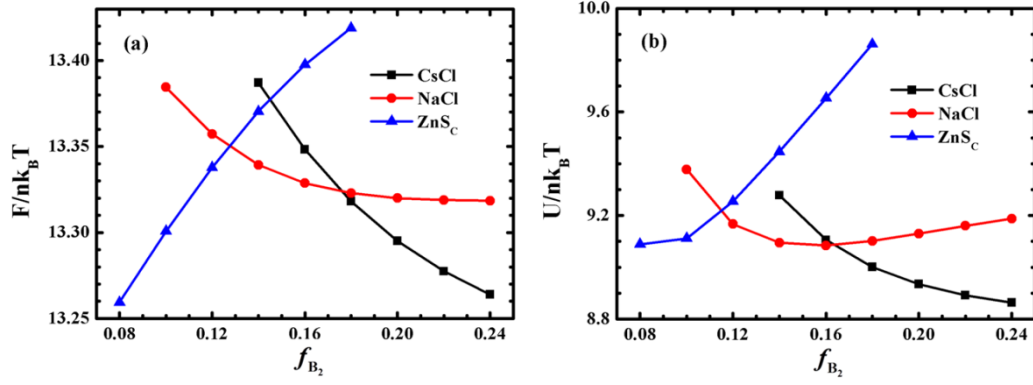


Fig. S1.

Energy comparisons between CsCl, NaCl, ZnS_C phases for B₁AB₂CB₁ terpolymers with fixed $\chi N = 80$ and $f = 0.10$. Figures (a) and (b) are the free energy and the interfacial energy, respectively.

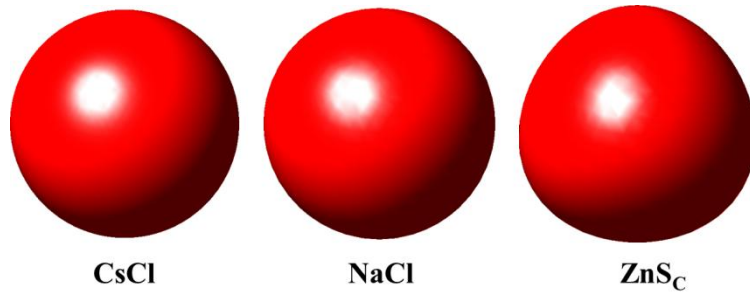


Fig. S2.

Isosurface plots of A-sphere at $\phi_A(\mathbf{r}) = 0.5$ of three crystal phases CsCl, NaCl, and ZnS_C for B₁AB₂CB₁ terpolymers with $f_{B_2} = 0.18$, $\chi N = 80$ and $f = 0.10$. From left to right, the deformation from ideal sphere becomes more and more noticeable.

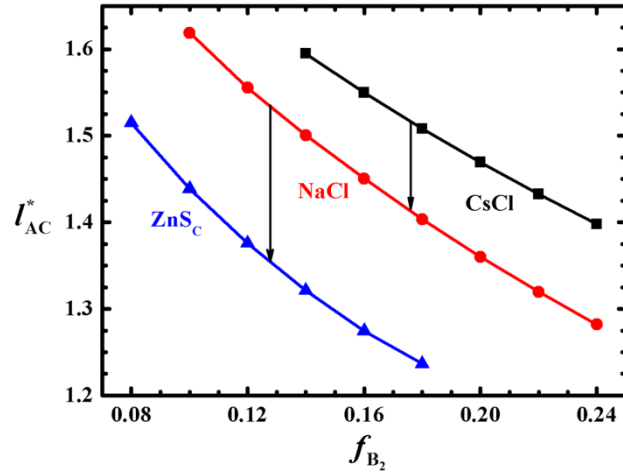


Fig. S3.

Variation of the A-C sphere distance, which is divided by the ideal end-to-end distance between the centers of A and C blocks, $l_0 = [(f_{B_2} + f)N]^{1/2}b$, for $B_1AB_2CB_1$ terpolymers with fixed $\chi N = 80$ and $f = 0.10$. The arrows indicate the transitions between these phases.

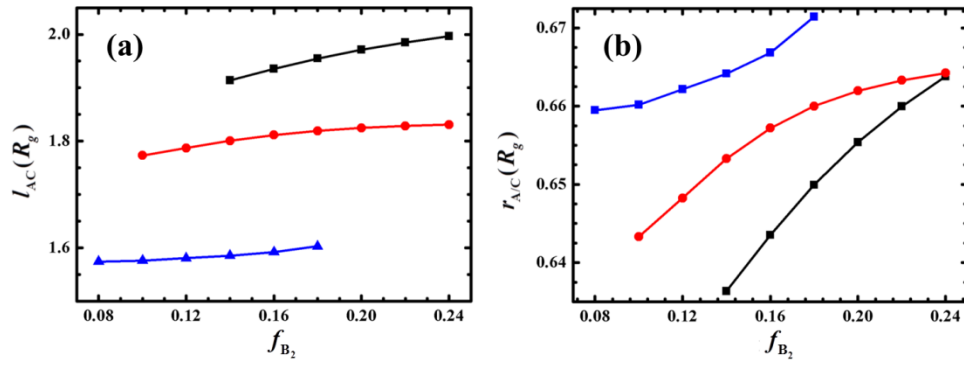


Fig. S4.

(a) A-C sphere distance and (b) the radius of spheres as a function of f_{B_2} for $B_1AB_2CB_1$ terpolymers with fixed $\chi N = 80$ and $f = 0.10$. The sphere radius is estimated under the strong-segregation approximation and the assumption that the domain shape is ideally

spherical. Symbols in black, red, and blue colors indicate the results of CsCl, NaCl, and ZnS_C phases, respectively.

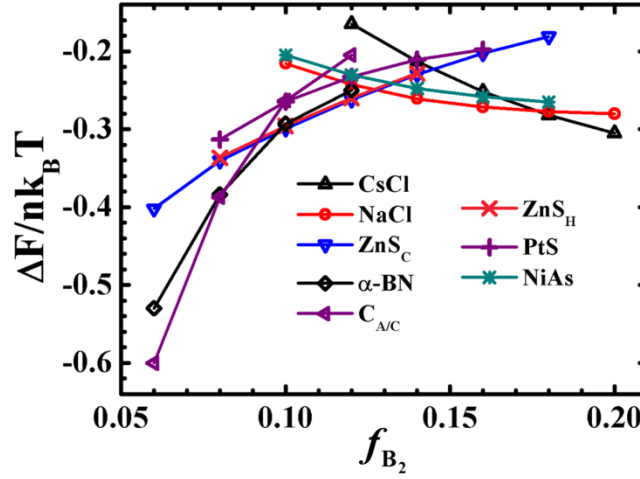


Fig. S5

Free energy comparison between candidate phases for symmetric B₁AB₂CB₁ terpolymers with fixed $\chi N = 80$ and $f = 0.10$. This comparison indicates that the stable phase sequence for reducing f_{B_2} is CsCl, NaCl, ZnS_C, α -BN, and C_{A/C}, and the other phases, including NiAs, ZnS_H, and PtS, are metastable. Note that, there are two intriguing features. One is that the hexagonal phase of ZnS_H has consistently higher free energy than the cubic phase of ZnS_C, but the free energy difference per chain is as tiny as $10^{-3} k_B T$. The other feature is that the non-cubic (tetragonal) phase of NiAs with the same CN of 6 as the cubic phase of NaCl has noticeable higher free energy, and that the non-cubic (tetragonal) phase of PtS with the same CN of 4 as ZnS_C has fairly higher free energy. This suggests that the cubic phases are preferred to the non-cubic phases under the situation of same CNs for symmetric block terpolymers with the present parameters, *i.e.*, equal interaction parameters and equal segment sizes. Further studies are required to

explore the stability of non-cubic phases relative to cubic phases in other situations of parameters.

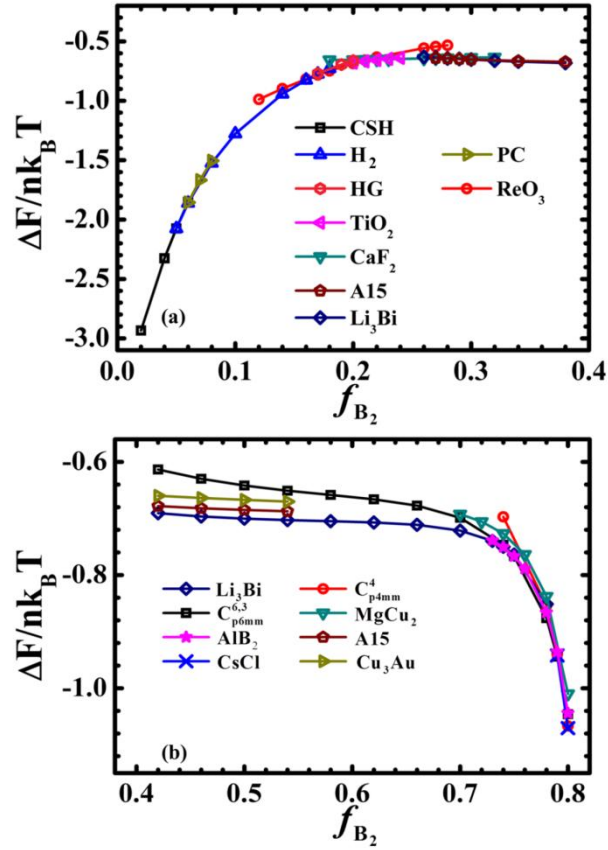


Fig. S6

Free energy comparison between candidate phases for complete asymmetric AB_2CB_3 terpolymers with fixed $\chi N = 80$ and $f = 0.09$. For the reason of clarity, these free energy data with $0 < f_{B_2} \leq 0.4$ and $0.4 < f_{B_2} \leq 0.8$, are plotted into two figures, (a) and (b), respectively. This comparison reveals that the stable phase sequence is CsCl, $C_{p6mm}^{6,3}$, Li_3Bi , Nb_3Sn (A15), CaF_2 , TiO_2 , ReO_3 , helical supercylinder of H_2 , and hexagonal core-shell cylinder of CSC. One non-cubic phase of TiO_2 with $\overline{CN} = 4$ is identified as stable phase located between two cubic phases of CaF_2 with $\overline{CN} = 16/3$ and ReO_3 with $\overline{CN} = 3$.

Different from the situation of the symmetric terpolymers in Fig. S2, two cubic metastable phases, MgCu_2 with $\overline{\text{CN}} = 8$ and Cu_3Au with $\overline{\text{CN}} = 6$, are examined. As increasing the length of end B-block from $f_{B_1} = 0$, where the stable phase is CsCl with $\overline{\text{CN}} = 8$, the average CN tends to decline, and the asymmetry of CNs is introduced. The two factors make MgCu_2 be less favorable than CsCl or other phase such as Li_3Bi , which in particular has a closer $\overline{\text{CN}} = 7$ to CsCl. Though Cu_3Au has the same $\overline{\text{CN}}$ and CN asymmetry as Nb_3Sn (A15), it still has higher free energy than the latter.

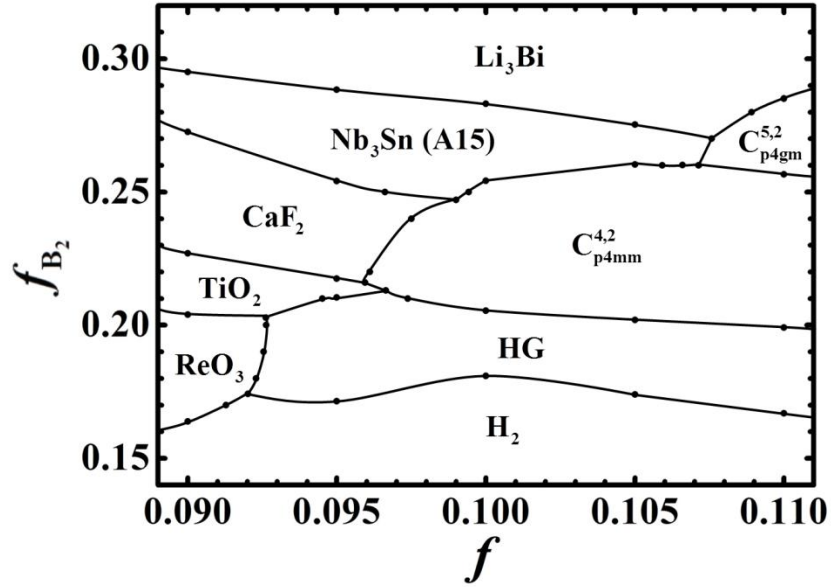


Fig. S7

Enlarged portion of the phase diagram in Fig. 3.

Table S4.

List of free energy data for the phases of Li_3Bi , A15, and $\text{C}_{\text{p4mm}}^{4,2}$ on the path of $f = 0.1$. in the phase diagram of Fig. S7. The lowest free energy is highlighted in bold. The data indicates that the free energy difference per chain near the phase boundary is as tiny as $10^{-3} k_{\text{B}}T$.

Phase f_{B_2}	0.24	0.25	0.26	0.27	0.28	0.29
C_{p4mm}^{4,2}	12.30514	12.31804	12.33185	—	—	—
A15	12.32835	12.32051	12.31358	12.30748	12.30208	12.29732
Li₃Bi	12.33776	12.32809	12.31901	12.31058	12.30282	12.29569

Reference

(S1) Xu, W. Q.; Jiang, K.; Zhang, P. W.; Shi, A. C. *J. Phys. Chem. B* **2013**, *117*, 5296-5305.